1 of 1

N75 21635

UNCLAS

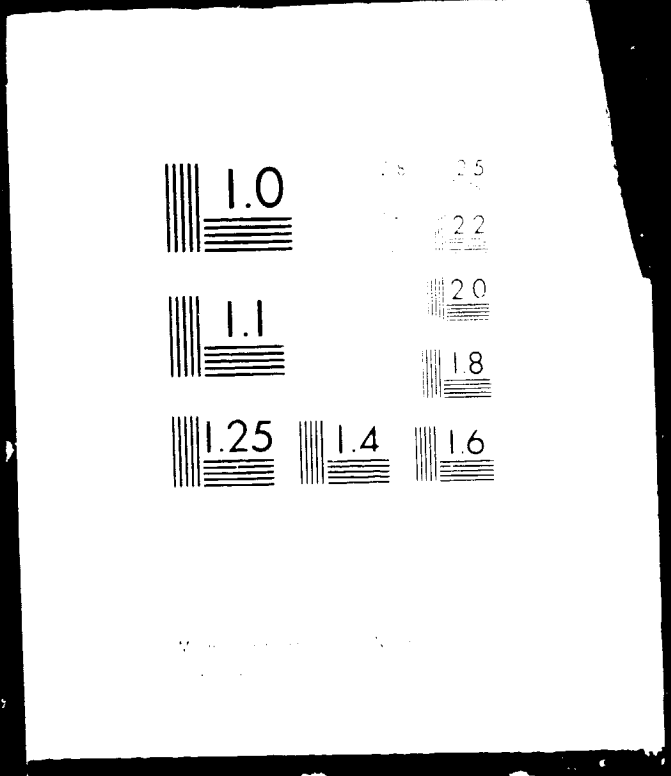

BIMONTHLY REPORT

RESEARCH STUDY ON STABILIZATION AND CONTROL

MODERN SAMPLED-DATA CONTROL THEORY

SYSTEMS RESEARCH LABORATORY

P.O. BOX 2277, STATION A
3206 VALLEY BROOK DRIVE
CHAMPAIGN, ILLINOIS 61820

PREPARED FOR GEORGE C. MARSHALL SPACE FLIGHT CENTER

HUNTSVILLE, ALABAMA

BI-MONTHLY REPORT

RESEARCH STUDY ON STABILIZATION AND CONTROL

– MODERN SAMPLED-DATA CONTROL THEORY

ANALYSIS AND DESIGN OF THE

DIGITAL LARGE SPACE TELESCOPE

SUBTITLE: SYSTEM

March 1, 1975 NAS8-29853

BY B.C. KUO
G. SINGH

PREPARED FOR GEORGE C. MARSHALL SPACE FLIGHT CENTER

HUNTSVILLE, ALABAMA

CONTRACT NAS8-29853 DCN 1-2-40-23018

SYSTEMS RESEARCH LABORATORY

P.O. BOX 2277, STATION A

CHAMPAIGN, ILLINOIS 61820

1. Pointing Accuracy of the Low-Cost Large Space Telescope Due to Noise and Quantization

1-1. Introduction

The objective of this study is to conduct an investigation on the pointing stability of the low-cost Large Space Telescope (LST) system. The low-cost LST is characterized by the use of reaction wheels for the generation of control torques. Because of the critical requirement on the pointing accuracy of the LST, the nonlinear frictional characteristics of the bearings of the reaction wheels cannot be neglected. It is well known that the nonlinear friction can cause limit cycles in a closed-loop system.

Another possible source of pointing error in the LST is due to the effect of quantization and sensor noise. Since the LST is a digital system, D-A and A-D converters, and sensors for positional and rate feedbacks are used. Sensor noise and amplitude quantization will also cause pointing error in the LST. In addition, quantization is a nonlinear phenomenon so that it may also cause self-sustained oscillations in the closed-loop system.

The dynamic modeling of the single-axis LST is described in this chapter. Several methods of evaluating the attitude error of the digital LST due to quantization and noise inputs are given.

1-2. Dynamic Models of the Low-Cost LST System

The dynamic model of the single-axis low-cost LST system with sampled data is shown in the block diagram of Fig. 1-1. The rigid body is represented by the double-integrator transfer function. The controller is formed by proportional, rate, and integral feedbacks of the vehicle attitude. The nonlinear element N in the reaction wheel dynamics represents the rolling friction, and its functional description is given by the well-known Dahl model.

The definitions of variables and the values of parameters and constants are tabulated in Table 1-1 [1].

Table 1-1.

ϕ_c	Reference input command	
ϕ_B	Body attitude of LST	
$\dot{\phi}_B$	Body rate of LST	
T_C	Torque command of reaction wheel	
T_{RW}	Torque output of reaction wheel	
$\dot{\theta}_{RW}$	Angular velocity of reaction wheel	
θ_{RW}	Angular displacement of reaction wheel	
T_F	Frictional torque of reaction wheel	
ϕ_e	Attitude error	
K_p	Proportional gain of controller	1.65×10^6 N-m/rad
K_R	Rate gain of controller	3.71×10^5 N-m/rad/sec
K_I	Integral gain of controller	7.33×10^5 N-m/rad/sec
R_F	Feedback resistance	0.484 ohms
K_A	Voltage amplifier gain	10000

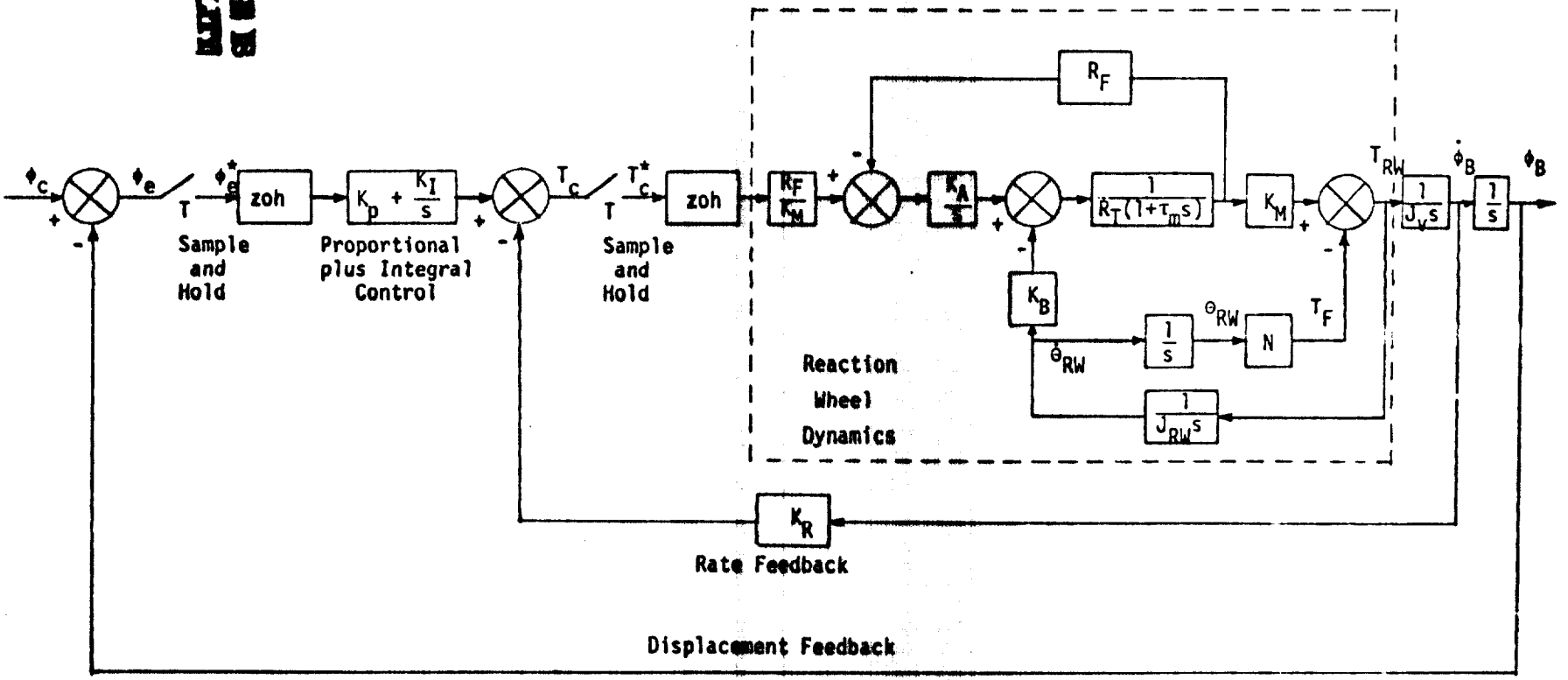

Figure 1-1. Digital low-cost LST system (single axis).

K_M	Motor torque constant	0.484 N-m/amp
K_B	Back emf constant	0.484 volt/rad/sec
J_{RW}	Moment of inertia of reaction wheel	0.2 Kg-m^2
J_v	Moment of inertia of vehicle about pitch axis	41822 Kg-m^2
τ_m	Motor time constant	0.002 sec
R_T	Motor resistance	10 ohms

Although the low-cost LST system has digital control, it is informative to analyze the system of Fig. 1-1 first without the sample-and-hold device. Figure 1-2 shows the signal flow graph of the continuous-data LST system. The characteristic equation of the system is determined from Fig. 1-2,

$$\Delta = 1 + R_F G_2 G_3 + K_B K_M G_3 G_6 + \frac{R_F K_M K_R}{K_M} G_2 G_3 G_4 + R_F G_1 G_2 G_3 G_4 G_5 \qquad (1\text{-}1)$$

where

$$G_1 = K_p + K_I/s$$

$$G_2 = K_A/s$$

$$G_3 = \frac{1}{R + (1 + \tau_m s)}$$

$$G_4 = \frac{1}{J_v s}$$

$$G_5 = \frac{1}{s}$$

$$G_6 = \frac{1}{J_{RW} s}$$

$$G_7 = \frac{1}{s}$$

and N denotes the analog describing function of the reaction wheel nonlinearity.

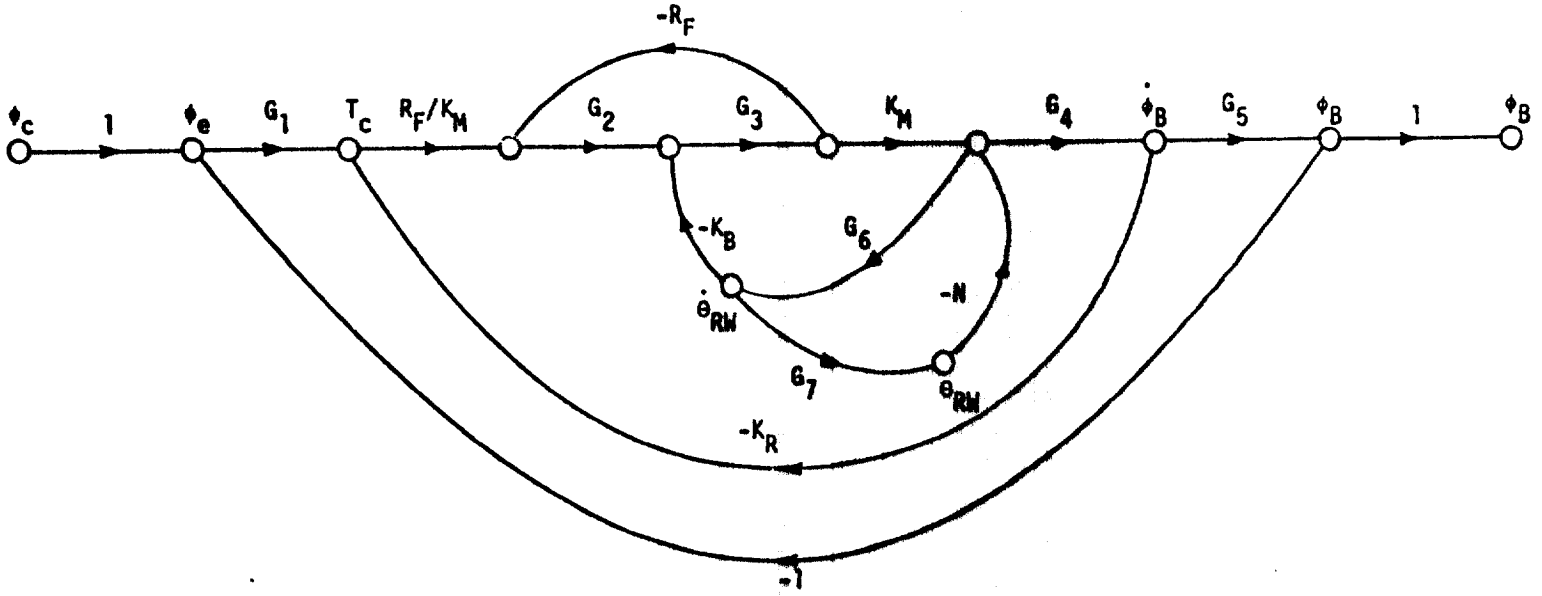

Figure 1-2. Signal flow graph of the continuous-data low-cost LST system.

For the linear model of the LST system, we set N = 0, and the characteristic equation becomes

$$\tau_m J_v R_T s^5 + J_v R_T s^4 + (J_v R_F K_A + \frac{K_B K_M J_v}{J_{RW}}) s^3 + R_F K_R K_A s^2 + K_A R_F K_p s + K_A K_I R_F = 0 \quad (1\text{-}2)$$

It is of interest to investigate the dynamics of the reaction wheel and the vehicle. The open-loop transfer function between T_c and ϕ_B is

$$\frac{\phi_B}{T_c} = \frac{R_F K_A}{J_v s^2 (R_T \tau_m s^2 + R_T s + R_F K_A + \frac{K_M K_B}{J_{RW}})} \quad (1\text{-}3)$$

Substituting the system parameters into Eq. (1-3) gives

$$\frac{\phi_B}{T_c} = \frac{5.7865}{s^2(s^2 + 500s + 242058.5)} = \frac{5.7865}{s^2(s + 250 + j423.74)(s + 250 + j423.74)} \quad (1\text{-}4)$$

Thus, the reaction wheel is shown to have relatively fast dynamics.

Substitution of the values of the system parameters into Eq. (1-2), and simplifying, the characteristic equation of the linear LST system is written

$$s^5 + 500s^4 + 242058.5s^3 + 2.1468 \times 10^6 s^2 + 9.5476 \times 10^6 s + 4.24145 \times 10^6 = 0 \quad (1\text{-}5)$$

The roots of the characteristic equation are:

$s = -0.49659$

$s = -4.22743 + j4.25123$

$s = -4.22743 - j4.25123$

$s = -245.524 + j421.118$

$s = -245.524 - j421.118$

Note that the damping ratio of the dominant complex roots is 0.705, and the natural undamped frequency is 6 rad/sec or 0.954 Hz. These parameters are achieved by selecting the controller constants K_p, K_R and K_I at the indicated values. However, the poles of the reaction wheel dynamics at $s = -250 + j423.74$ and $s = -250 - j423.74$ are only slightly affected by the body controller and they account for the characteristic roots at $s = -245.524 + j421.118$ and $s = -245.524 - j421.118$ of the overall closed-loop system. Since these fast roots are very far away from the dominant ones, this means that for all practical purposes the dynamics of the reaction wheel can be neglected as far as the linear system is concerned. Figure 1-3 shows the block diagram of the simplified continuous-data low-cost LST system, and the digital system is shown in Fig. 1-4.

The closed-loop transfer function of the continuous-data system of Fig. 1-3 is

$$\frac{\Phi_B(s)}{\Phi_c(s)} = \frac{K_p s + K_I}{J_v s^3 + K_R s^2 + K_p s + K_I} \tag{1-6}$$

For the digital system of Fig. 1-4, the closed-loop transfer function is written

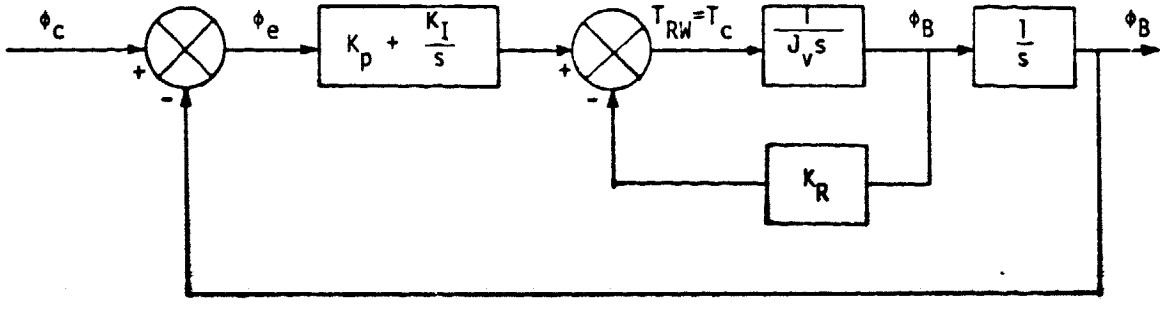

Figure 1-3. Simplified continuous-data low-cost LST system.

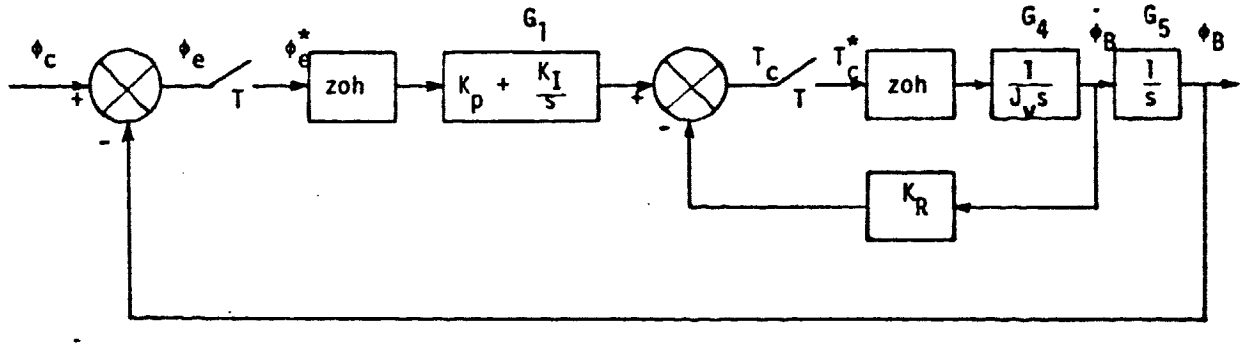

Figure 1-4. Simplified digital low-cost LST system.

$$\frac{\Phi_B(z)}{\Phi_c(z)} = \frac{G_A(z)G_B(z)}{1 + G_c(z) + G_A(z)G_B(z)} \tag{1-7}$$

where

$$G_{ho}(s) = \frac{1 - e^{-Ts}}{s}$$

$$G_A(z) = \mathcal{Z}(G_{ho}G_1) = (1 - z^{-1})\mathcal{Z}\left(\frac{K_I s + K_I}{s^2}\right) = \frac{K_p z + K_I T - K_p}{z - 1} \tag{1-8}$$

$$G_B(z) = \mathcal{Z}(G_{ho}G_4G_5) = (1 - z^{-1})\mathcal{Z}\left(\frac{1}{J_v s^3}\right) = \frac{T^2(z + 1)}{2J_v(z - 1)^2} \tag{1-9}$$

$$G_c(z) = \mathcal{Z}(G_{ho}G_4K_R) = K_R(1 - z^{-1})\mathcal{Z}\left(\frac{1}{J_v s^2}\right) = \frac{K_R}{J_v}\frac{T}{z - 1} \tag{1-10}$$

Equation (1-7) is simplified to

$$\frac{\Phi_B(z)}{\Phi_c(z)} = \frac{T^2(K_p z^2 + K_I T z + K_I T - K_p)}{2J_v z^3 + (T^2K_p + 2K_R T - 6J_v)z^2 + (6J_v - 4K_R T + T^2 K_I T)z + (2K_R T + K_I T^3 - 2J_v - K_p T^2)} \tag{1-11}$$

The characteristic equation of the system is

$$2J_v z^3 + (T^2K_p + 2K_R T - 6J_v)z^2 + (6J_v - 4K_R T + T^3 K_I)z + 2K_R T + K_I T^3 - 2J_v - K_p T^2 = 0 \tag{1-12}$$

Or,

$$83644z^3 + (1.65 \times 10^6T^2 + 7.42 \times 10^5T - 2.50932 \times 10^5)z^2$$
$$+ (2.50932 \times 10^5 - 14.84 \times 10^5T + 7.33 \times 10^5T^3)z$$
$$+ (-8.3644 \times 10^4 + 7.42 \times 10^5T + 7.33 \times 10^5T^3 - 1.65 \times 10^6T^2) = 0 \quad (1\text{-}13)$$

The characteristic equation roots are tabulated below as functions of the sampling period T:

T (msec)	Roots
0.1	1, 0.998 ± j0.0025
0.5	1, 0.998 ± j0.0022
1	1, 0.996 ± j0.0043
5	0.998, 0.979 ± j0.0208
10	0.995, 0.957 ± j0.0411
25	0.987, 0.889 ± j0.0988
50	0.975, 0.766 ± j0.1825
100	0.950, 0.483 ± j0.2901
120	0.940, 0.356 ± j0.300
150	0.925, 0.150 ± j0.260
170	0.915, 0.0034 ± j0.144
180	0.910, 0.049, -0.195
200	0.900, 0.107, -0.571
220	0.890, 0.1116, -0.9078
230	0.885, 0.1085, -1.077 (unstable)

The root loci of Eq. (1-13) are sketched in Fig. 1-5 as a function of T. For small sampling periods, the characteristic roots are all located near

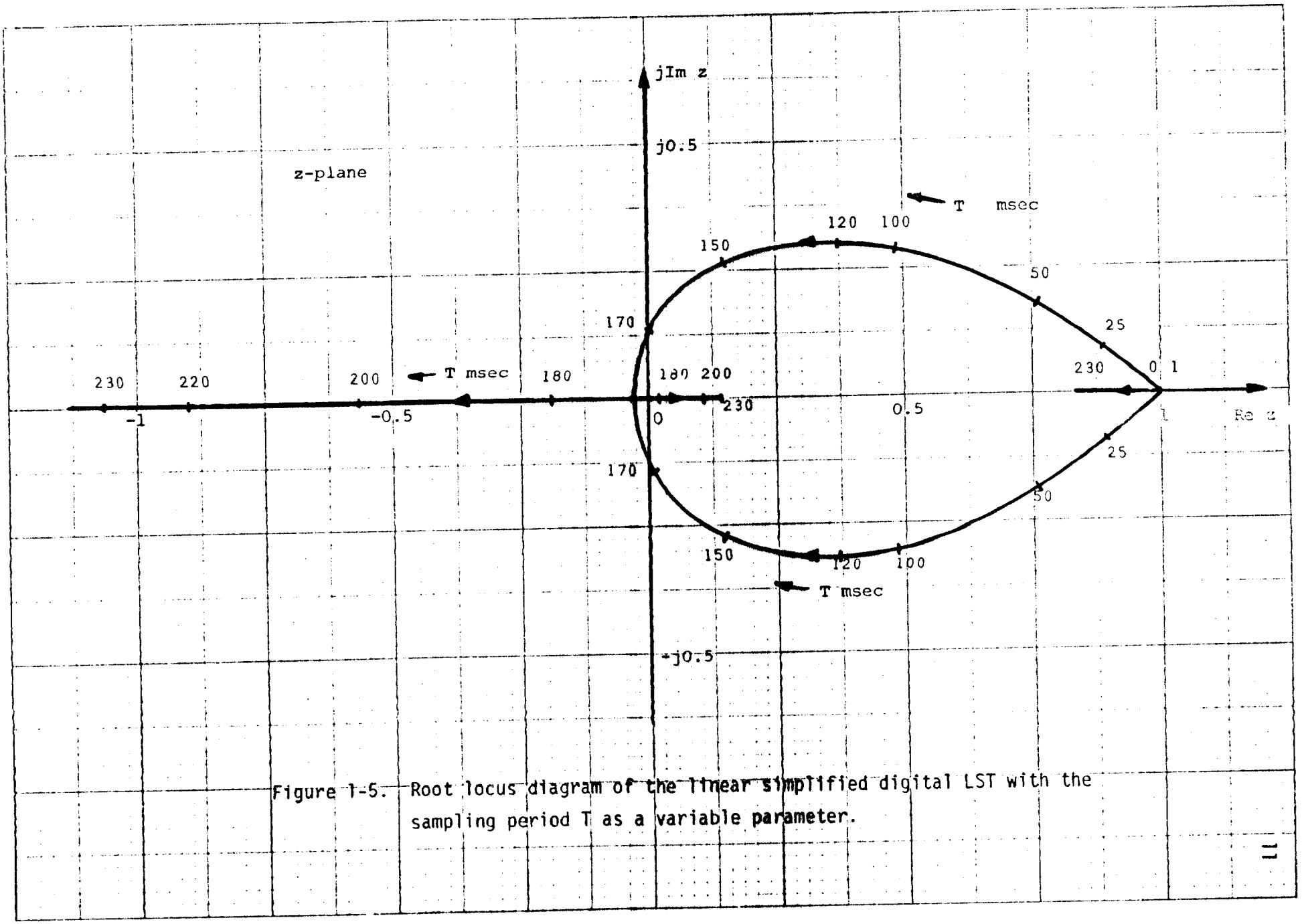

Figure 1-5. Root locus diagram of the linear simplified digital LST with the sampling period T as a variable parameter.

the $z = 1$ point. The linear digital LST system becomes unstable when T exceeds approximately 225 msec.

1-3. Effects of Quantization on Pointing Stability of the Low-Cost LST - Limit Cycle Conditions

Quantization occurs at at least three places in the LST system. Two are at the displacement sensor and the rate sensor where A-to-D converters are used. A quantizer is also needed at the control torque input to the reaction wheel since D-to-A conversion is effected there. In addition, if the integral control K_I/s is implemented digitally, quantization should be considered in the digital controller as well. Figure 1-6 shows the digital LST system with quantizers. The z-transfer functions are defined in Eqs. (1-8), (1-9), and (1-10). The quantizers at the displacement sensor, the rate sensor, and the reaction wheel control torque are denoted by Q_p, Q_R, and Q_T, respectively. The input-output relation of a quantizer is shown in Fig. 1-7. The quantization level is represented by h.

We shall analyze the effects of quantization on pointing stability or accuracy of the LST by means of three different methods. The first method utilizes the deterministic approach and establishes a least upper bound on the pointing error due to quantization. The second method relies on treating the quantizer as a noise source, and statistical analysis is applied. The third method is also a statistical approach which represents the quantizer by a linearized gain $K_{eq}(z)$.

It should be pointed out that a system with quantization is a nonlinear system and its behavior cannot be predicted by linear theory. One of the well-known phenomena of a nonlinear system is that sustained oscillations may occur. When a digital system has several quantizers, it is extremely difficult to predict the condition of self-sustained oscillations.

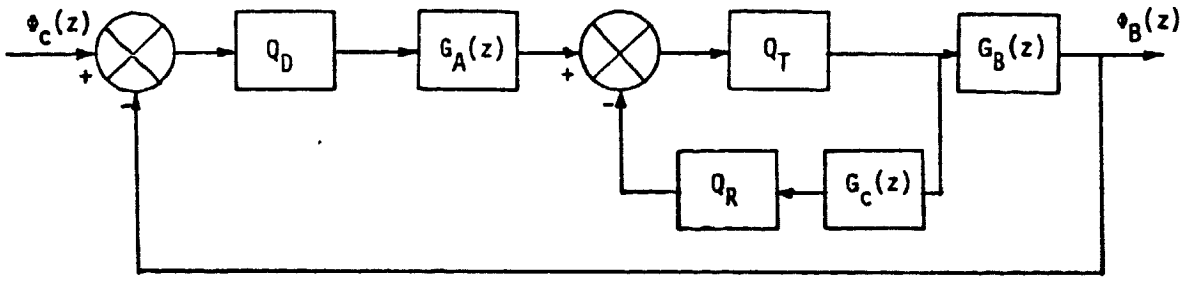

Figure 1-6. Simplified digital LST system with quantizers.

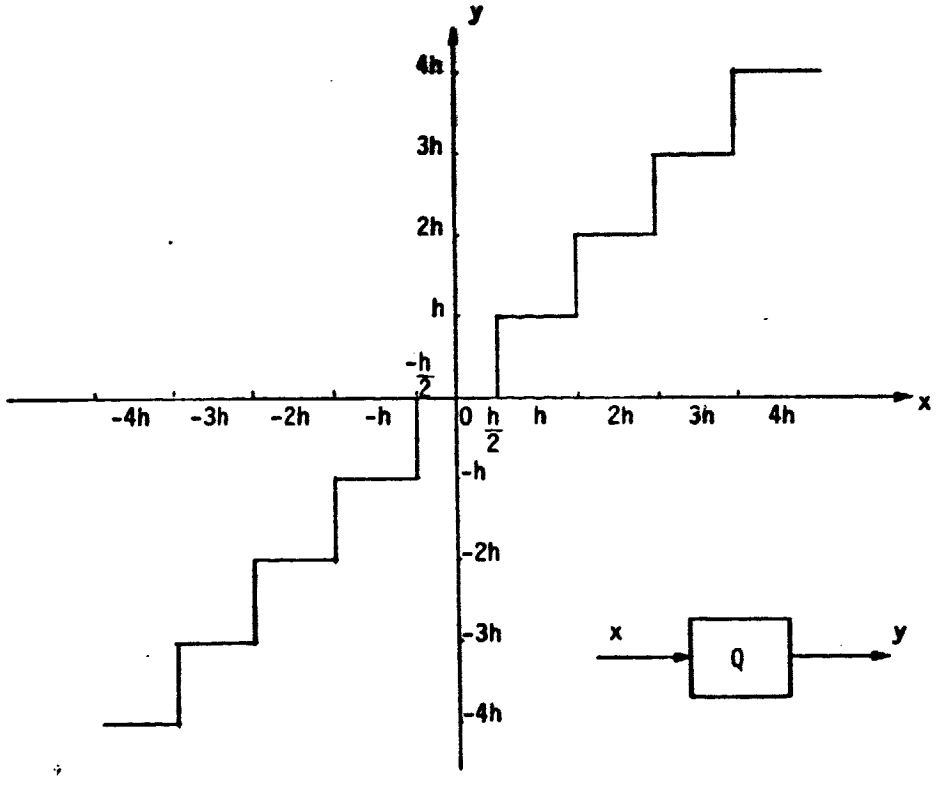

Figure 1-7. Input-output characteristics of a quantizer.

To illustrate the effects of quantization, and how quantization can cause sustained oscillations in an otherwise stable linear system, let us refer to the digital systems shown in Figs. 1-8 and 1-9. The difference between the two systems in Figs. 1-8a and 1-9a is that the former has negative feedback and the latter has positive feedback; but both systems are stable.

For $r(k) = 0$, both linear systems have zero steady-state values for $c(k)$; that is, $c(k) = 0$ for $k \to \infty$, for arbitrary initial state $c(0)$. We shall show that when quantization is considered, the system in Fig. 1-9b has a steady-state error, whereas the system in Fig. 1-8b exhibits a sustained oscillation.

Let the quantization level h be 2, (Fig. 1-7). The state equation of the system in Fig. 1-9b is

$$c(k+1) = Q[0.9c(k)] \tag{1-14}$$

For $c(0) = 10$, it can be easily shown that $c(k) = 2$ for $k \geq 8$.

The state equation of the system in Fig. 1-8b is

$$c(k+1) = Q[-0.9c(k)] \tag{1-15}$$

For $c(0) = 10$, $c(k) = 2$ for $k \geq 8$ even, and $c(k) = -2$ for $k > 8$ odd. Thus, the state of the system oscillates between -2 and +2.

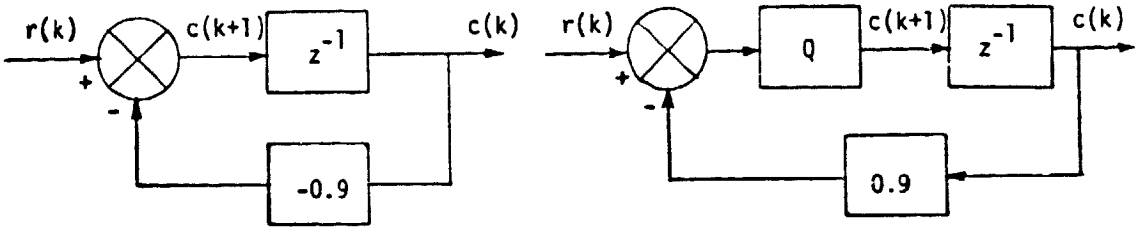

(a) Linear system (b) System with quantizer

Figure 1-8. Systems with quantizers.

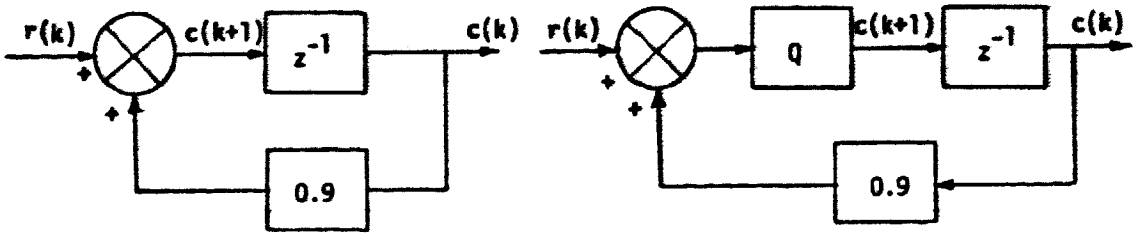

(a) Linear system (b) System with quantizer

Figure 1-9. Systems with quantizers.

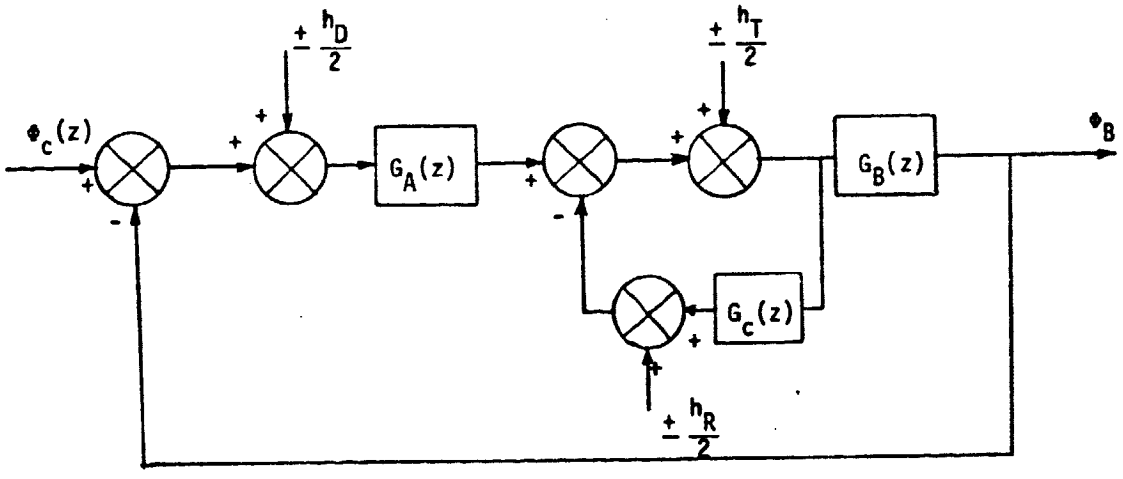

Figure 1-10. Digital LST system with quantizers replaced by deterministic noise sources.

1-4. Effects of Quantization on Pointing Stability of the Digital Low-Cost LST - Least Upper Bound Quantization Error

In this section the effects of quantization on the low-cost LST system are investigated using a deterministic approach. The method of analysis is based on the "worst" error condition due to quantization. In general, the analysis gives a conservative estimation of the quantization error.

Since the quantization error has a maximum bound of $\pm h/2$, the "worst" error due to quantization in a digital system can be studied by replacing the quantizer in the state diagram by a branch with unity gain and an external noise source with a signal magnitude of $\pm h/2$. The block diagram of the digital LST system with quantizers shown in Fig. 1-6 is redrawn in Fig. 1-10 with the noise sources. The transfer functions $G_A(z)$, $G_B(z)$, and $G_c(z)$ are defined in Eqs. (1-8), (1-9), and (1-10), respectively.

The z-transform of the body attitude of the LST due to the three quantizers when $\phi_c = 0$ is

$$\Phi_B(z) = \frac{z}{z-1} \frac{\pm \frac{h_D}{2} G_A(z) \pm \frac{h_T}{2} \pm \frac{h_R}{2}}{1 + G_A(z)G_B(z) + G_c(z)} G_B(z) \tag{1-16}$$

Substitution of Eqs. (1-8) through (1-10) into Eq. (1-16), and simplifying, we have

$$\Phi_B(z) = \frac{z}{z-1} \frac{[\pm \frac{h_D}{2}(K_D z + K_I T - K_p) \pm (\frac{h_T}{2} + \frac{h_R}{2})(z-1)]T^2(z+1)}{2J_v(z-1)^3 + T^2(z+1)(K_p z + K_I T - K_p) + 2TK_R(z-1)^2} \tag{1-17}$$

The steady-state error of the body attitude due to the quantization effects is obtained by applying the final-value theorem to Eq. (1-17), (if the system is stable).

Thus,

$$\lim_{k\to\infty} \Phi_B(kT) = \lim_{z\to 1} (1 - z^{-1})\Phi_B(z) = \pm \frac{h_D}{2} \tag{1-18}$$

It is interesting to explore the significance of this result on the error due to quantization. Firstly, the quantization error at the displacement sensor is propagated through the system without change in amplitude. Secondly, the errors due to the torque and rate sensor quantizers are completely eliminated at the output position. This is attributed to the integral control K_I/s in the forward path.

Digital Implementation of Forward Controller

If the proportional-plus-integral controller is implemented digitally, the transfer function $G_A(z)$ becomes

$$G_A(z) = K_p + \frac{TK_I(z + 1)}{2(z - 1)} \tag{1-19}$$

Substituting $G_A(z)$ from Eq. (1-19) into Eq. (1-16), we can again show that the steady-state error in $\Phi_B(kT)$ due to the three quantizers is $\pm h_D/2$, and the errors due to Q_R and Q_T are completely eliminated.

In reality, the digital implementation of the controller should also include quantization in the digital process. Figure 1-11 shows the block diagram of the LST system with quantizations also considered in the digital controller. The z-transform of the body attitude of the

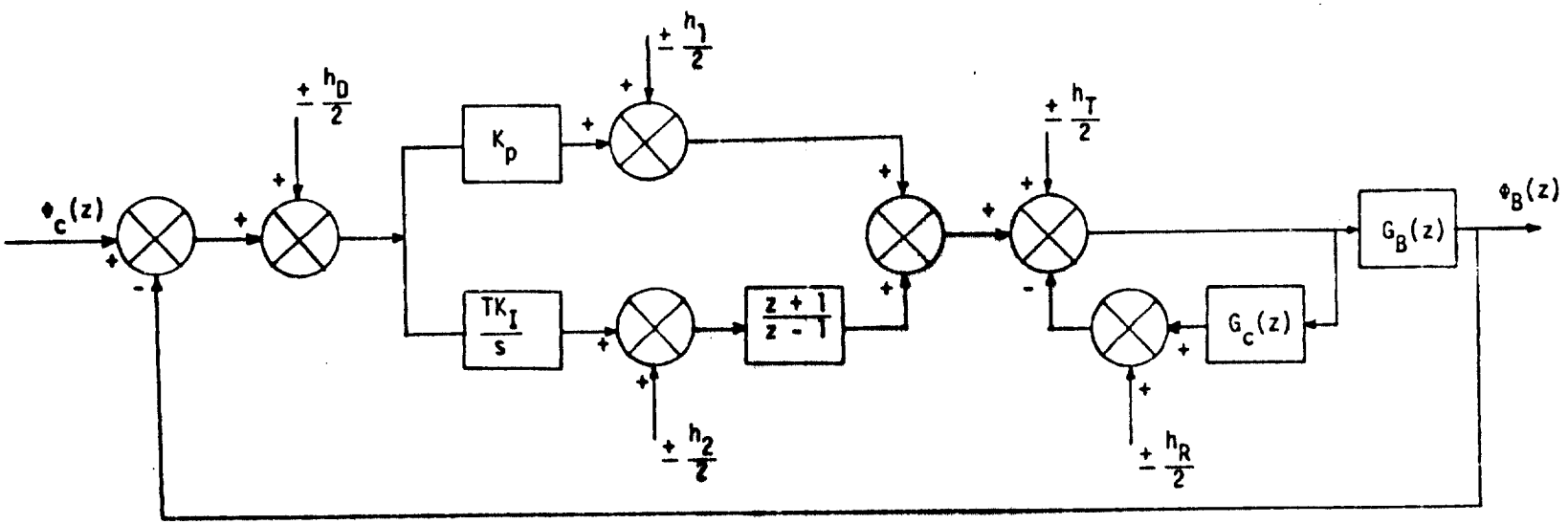

Figure 1-11. Digital LST system with quantizers in the digital controller.

LST due to the five quantizers when $\theta_c = 0$ is

$$\Phi_B(z) = \frac{4}{z-1} \frac{\pm\frac{h_D}{2} G_A(z) \pm \frac{h_1}{2} \pm \frac{h_2}{2}\left(\frac{z+1}{z-1}\right) \pm \frac{h_R}{2} \pm \frac{h_T}{2}}{1 + G_A(z)G_B(z) + G_c(z)} G_B(z) \qquad (1\text{-}20)$$

where $G_A(z)$ is given by Eq. (1-19) and $G_B(z)$ and $G_c(z)$ are given in Eqs. (1-9) and (1-10), respectively.

Applying the final-value theorem to Eq. (1-20), we have

$$\lim_{k\to\infty} \Phi_B(kT) = \frac{\pm h_2 \pm h_D K_I T}{2K_I T} = \pm\frac{h_D}{2} \pm \frac{h_2}{2K_I T} \qquad (1\text{-}21)$$

It is interesting to note that the introduction of the integral control eliminates the noise signals that enter at all points after the integral control in the control loop; however, the digital implementation of this control in turn produces a quantization error which is bounded by $\pm h_2/2K_I T$, where h_2 is the quantization level.

1-5. Effects of Quantization on Pointing Stability of the Digital Low-Cost LST - Equivalent Noise Source, Statistical Analysis

In this section the pointing errors of the digital LST system due to quantizations in the displacement, rate, and torque channels are investigated by statistical means. The rms (root-mean-square) error in ϕ_B due to quantizations that are represented by equivalent Gaussian noise sources with zero mean, or white noise sources, is determined by setting $\phi_c = 0$. The results are then compared with those of the continuous-data LST obtained in reference [1].

The block diagram model of the continuous-data LST with the quantizers replaced by equivalent noise sources is shown in Fig. 1-12. The equivalent digital system is shown in Fig. 1-13. It is assumed that the equivalent noise sources that represent the quantization operations are white, so that their power spectral density functions in both the s and the z domains are constants. Therefore,

$\Phi_D(s)$, $\Phi_D(z) = \Phi_D$ = power spectral density of displacement quantizer

$\Phi_R(s)$, $\Phi_R(z) = \Phi_R$ = power spectral density of rate quantizer

$\Phi_T(s)$, $\Phi_T(z) = \Phi_T$ = power spectral density of rate quantizer

Let the rms attitude error of the continuous-data LST due to Φ_D be represented by σ_{BD}. The rms errors are given by the following relations:

Displacement:

$$\sigma_{BD} = \left[\frac{1}{2\pi j}\int_{-j\infty}^{j\infty} M_D(s)M_D(-s)ds \cdot \Phi_D\right]^{1/2} \qquad (1\text{-}22)$$

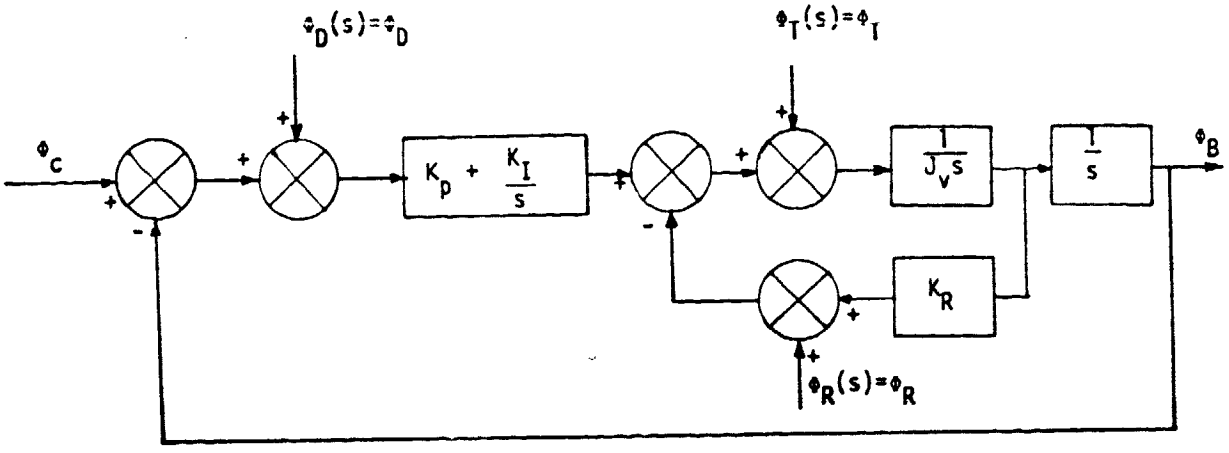

Figure 1-12. Continuous-data LST with quantizers represented by equivalent white noise sources.

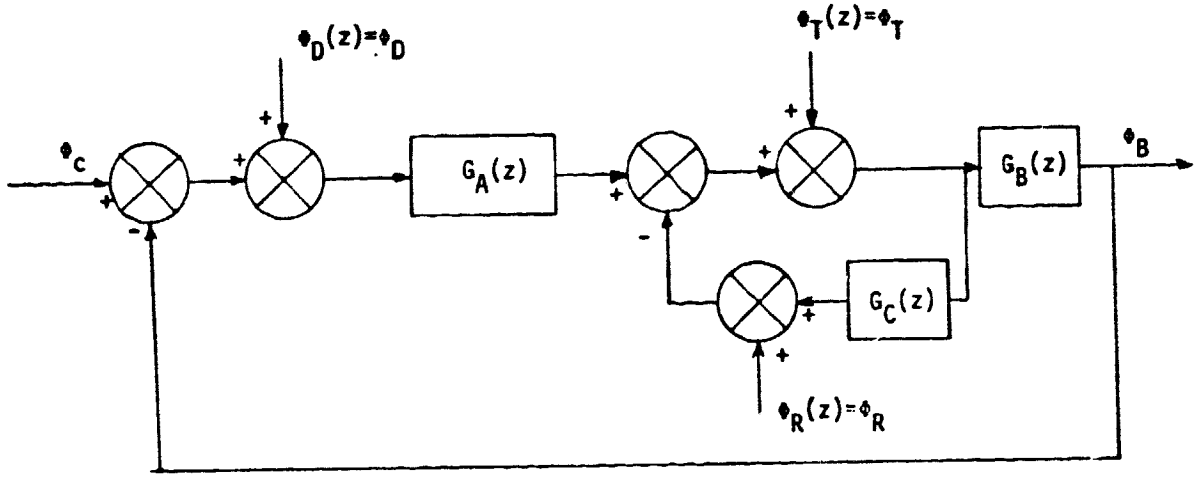

Figure 1-13. Digital LST with quantizers represented by equivalent white noise sources.

where $M_D(s)$ denotes the transfer function between $\Phi_D(s)$ and $\Phi_B(s)$,

$$M_D(s) = \frac{\Phi_B(s)}{\Phi_c(s)} = \frac{K_p s + K_I}{J_v s^3 + K_R s^2 + K_p s + K_I} \tag{1-23}$$

Similarly,

Rate:

$$\sigma_{BR} = \left[\frac{1}{2\pi j}\int_{-j\infty}^{j\infty} M_R(s)M_R(-s)ds \cdot \Phi_R\right]^{1/2} \tag{1-24}$$

Torque:

$$\sigma_{BT} = \left[\frac{1}{2\pi j}\int_{-j\infty}^{j\infty} M_T(s)M_T(-s)ds \cdot \Phi_T\right]^{1/2} \tag{1-25}$$

where

$$-M_R(s) = M_T(s) = \frac{\Phi_B(s)}{\Phi_T(s)} = \frac{s}{J_v s^3 + K_R s^2 + K_p s + K_I} \tag{1-26}$$

This result is obtained with the assumption that the quantizer noise is not multiplied by the sensor gain K_R, as in reference [1]; otherwise, the right-hand side of Eq. (1-26) should be multiplied by K_R.

The total rms attitude error due to all three quantizers is simply the sum of the errors due to each noise source acting alone; that is,

$$\sigma_B = \sigma_{BD} + \sigma_{BR} + \sigma_{BT} \tag{1-27}$$

From Eq. (1-26) it is easy to see that σ_{BR} and σ_{BT} have the same magnitude.

The line integral of the form of Eq. (1-22) can be evaluated by

contour integration, and then the residue theorem. An integral table is also available for the evaluation of the contour integral. Using Eqs. (1-23) and (1-26), the rms attitude errors of the continuous-data system are obtained as

$$\sigma_{BD} = \left(\frac{K_p^2 + K_I K_R}{2(K_R K_p - K_I J_v)} \Phi_D \right)^{1/2} = (2.5748\Phi_D)^{1/2} = 1.605\sqrt{\Phi_D} \tag{1-28}$$

$$\sigma_{BT} = \left(\frac{1}{2(K_R K_p - K_I J_v)} \Phi_T \right)^{1/2} = (0.8598 \times 10^{-12}\Phi_T)^{1/2}$$

$$= 0.927 \times 10^{-6}\sqrt{\Phi_T} \tag{1-29}$$

$$\sigma_{BR} = 0.927 \times 10^{-6}\sqrt{\Phi_R} \tag{1-30}$$

For the digital LST, the rms attitude errors are:

Displacement:

$$\sigma^*_{BD} = \left(\frac{1}{2\pi j} \oint M_D(z) M_D(z^{-1}) z^{-1} dz \cdot \Phi_D \right)^{1/2} \tag{1-31}$$

Rate:

$$\sigma^*_{BR} = \left(\frac{1}{2\pi j} \oint M_R(z) M_R(z^{-1}) z^{-1} dz \cdot \Phi_R \right)^{1/2} \tag{1-32}$$

Torque:

$$\sigma^*_{BT} = \left(\frac{1}{2\pi j} \oint M_T(z) M_T(z^{-1}) z^{-1} dz \cdot \Phi_T \right)^{1/2} \tag{1-33}$$

The transfer functions, $M_D(z)$, $M_R(z)$, and $M_T(z)$ are determined from

Fig. 1-13.

$$M_D(z) = \frac{G_A(z)G_B(z)}{1 + G_A(z)G_B(z) + G_c(z)} \tag{1-34}$$

$$-M_R(z) = M_T(z) = \frac{G_B(z)}{1 + G_A(z)G_B(z) + G_c(z)} \tag{1-35}$$

where

$$G_B(z) = \frac{T^2(z + 1)}{2J_v(z - 1)^2} \tag{1-36}$$

$$G_c(z) = \frac{K_R T}{J_v(z - 1)} \tag{1-37}$$

and

$$G_A(z) = \frac{K_p z + K_I T - K_p}{z - 1} \quad \text{(sample-and-hold and analog controller)} \tag{1-38}$$

$$G_A(z) = \frac{(2K_p + TK_I)z + TK_I - 2K_p}{2(z - 1)} \quad \text{(digital implementation of controller)} \tag{1-39}$$

Substituting Eqs. (1-36) through (1-39) into Eqs. (1-34) and (1-35), we get the following transfer functions which are used for the computation of the rms attitute errors in Eqs. (1-31) through (1-33).

With zero-order hold and analog controller,

$$M_D(z) = \frac{T^2[K_p z^2 + K_I z + (K_I T - K_p)]}{\Delta_1} \tag{1-40}$$

$$-M_R(z) = M_T(z) = \frac{T^2(z^2 - 1)}{\Delta_1} \tag{1-41}$$

where

$$\Delta_1 = 2J_v z^3 + (-6J_v + 2K_R T + T^2 K_p)z^2 + (6J_v - 4K_R T + K_I T^3)z + (-2J_v + 2K_R T + K_I T^3 - K_p T^2) \tag{1-42}$$

With digitally implemented controller,

$$M_D(z) = \frac{T^2[(2K_p + TK_I)z^2 + 2TK_I z + TK_I - 2K_p}{\Delta_2} \tag{1-43}$$

$$-M_R(z) = M_T(z) = \frac{2T^2(z^2 - 1)}{\Delta_2} \tag{1-44}$$

where

$$\Delta_2 = 4J_v z^3 + (-12J_v + 2T^2 K_p + T^3 K_I + 4K_R T)z^2 + (12J_v + 2T^3 K_I - 8K_R T)z + (4K_R T + T^3 K_I - 2T^2 K_p - 4J_v) \tag{1-45}$$

A tabulation method or a numerical method [3] can be used to evaluate the contour integrals of Eqs. (1-31), (1-32), and (1-33), once the values of the parameters of the transfer functions are known. Table 1-2 gives the values of $(\phi_{B\,rms})^*_D$, $(\phi_{B\,rms})^*_T$ and $(\phi_{B\,rms})^*_R$ for various values of the sampling period T.

Table 1-2.

T (msec)	Sample-and-Hold with Analog Controller		Digitally Implemented Controller	
	$\frac{\sigma^*_{BD}}{\sqrt{\Phi_D}}$	$\frac{\sigma^*_{BT}}{\sqrt{\Phi_T}}$	$\frac{\sigma^*_{BD}}{\sqrt{\Phi_D}}$	$\frac{\sigma^*_{BT}}{\sqrt{\Phi_T}}$
0.01	0.0052	2.932×10^{-9}	0.0052	2.932×10^{-9}
0.1	0.0161	9.274×10^{-9}	0.0161	9.274×10^{-9}
1.0	0.0508	2.936×10^{-8}	0.0508	2.936×10^{-8}
5.0	0.1140	6.599×10^{-8}	0.1141	6.595×10^{-8}
10	0.1621	9.394×10^{-8}	0.1622	9.383×10^{-8}
25	0.2602	1.515×10^{-7}	0.2607	1.511×10^{-7}
50	0.3777	2.216×10^{-7}	0.3796	2.205×10^{-7}
100	0.5652	3.368×10^{-7}	0.5720	3.339×10^{-7}

The results tabulated in Table 1-2 show that the rms errors of the LST with sample-and-hold and the analog controller are very close to those of the LST with the controller implemented digitally.

It is interesting to show that the rms attitude errors of the digital LST due to quantization are related to those of the continuous-data system in Fig. 1-12.

Applying the limit as T approaches zero to Eq. (1-31), we get

$$\lim_{T\to 0} \sigma^*_{BD} = \lim_{T\to 0} \left[\frac{1}{2\pi j}\oint M_D(z)M_D(z^{-1})z^{-1}dz\Phi_D\right]^{1/2} \tag{1-46}$$

Since

$$\lim_{T\to 0} M_D(z) = M_D(s) \tag{1-47}$$

where $M_D(s)$ is given in Eq. (1-23), and $M_D(z)$ is given by either Eq. (1-40) or (1-43), depending on the way the controller is implemented, and

$$z^{-1}dz = T\,ds \tag{1-48}$$

Eq. (1-46) is written

$$\lim_{T\to 0} \sigma^*_{BD} = \left[\frac{T}{2\pi j}\int_{-j\infty}^{j\infty} M_D(s)M_D(-s)ds\Phi_D\right]^{1/2} = \sqrt{T}\,\sigma_{BD} \tag{1-49}$$

or

$$\sigma_{BD} = \frac{1}{\sqrt{T}} \lim_{T\to 0} \sigma^*_{BD} \tag{1-50}$$

The meaning of this relation is that the mean-square value of the attitude error of the continuous-data system is equal to 1/T times the attitude error of the digital system as T approaches zero. Table 1-3 gives the values of $\sigma^*_{BD}/\sqrt{T\Phi_D}$ and $\sigma^*_{BT}/\sqrt{T\Phi_T}$ for various values of T. These values are very close to the values of $\sigma_{BD} = 1.605$ and $\sigma_{BT} = 0.926 \times 10^{-6}$, respectively, especially at very small sampling periods.

These relations show that, in general, for small sampling periods, the attitude error due to a white noise input in a digital system will be less than that of the same system without sampling. For example, for T = 25 msec, the rms attitude error σ^*_{BD} is $0.2602\sqrt{\Phi_D}$, whereas σ_{BD} is $1.605\sqrt{\Phi_D}$. Therefore, the use of the continuous-data LST model of Fig. 1-12, as in [1], for the error analysis of the digital LST results in conservative results.

Table 1-3.

T (msec)	$\frac{\sigma^{\star}_{BD}}{\sqrt{T\Phi_D}}$	$\frac{\sigma^{\star}_{BT}}{\sqrt{T\Phi_T}}$
0.01	1.644	0.927×10^{-6}
0.1	1.610	0.927×10^{-6}
1.0	1.606	0.928×10^{-6}
5.0	1.612	0.933×10^{-6}
10	1.621	0.939×10^{-6}
25	1.645	0.958×10^{-6}
50	1.689	0.991×10^{-6}
100	1.787	1.065×10^{-6}

The results in Tables 1-2 and 1-3 again show that for the same quantization levels, the quantizer in the displacement channel produces far greater attitude errors than those due to the quantizers in the rate and torque channels.

1-6. Effects of Quantization on Pointing Stability of the Digital Low-Cost LST - Quasilinear Analysis, Statistical

In this section the effects of quantization on the low-cost LST are studied by means of a quasilinearized equivalent-gain approach [4], [5]. Although the analysis is conducted in the statistical sense, there is a basic difference between the present analysis and the one conducted in Section 1-5. In the previous section, the rms attitude error of the LST is evaluated by treating the quantizers as noise sources that are stationary Gaussian processes with zero means. In this section, the quantizer will be treated as a nonlinear element whose input is a random stochastic process. An equivalent gain, $K_{eq}(z)$, is derived for the quantizer. The attitude of the LST is then determined with the quantizer replaced by $K_{eq}(z)$, and when the system is subject to a stochastic input. The only restriction with this method is that only one quantizer can be considered at a time. Since it has been established that the attitude of the LST is more sensitive to the quantizer Q_D, we shall consider only the system model shown in Fig. 1-14.

The quantizer Q_D is isolated as shown by the block diagram in Fig. 1-15a; the input is x(t) and the output is y(t). Figure 1-15b shows the equivalent gain representation of Q_D. The equivalent gain of Q_D is defined as

$$K_{eq}(z) = \frac{\Phi_{xy}(z)}{\Phi_{xx}(z)} \tag{1-51}$$

where $\Phi_{xx}(z)$ denotes the z-transform of the autocorrelation function of x(t), and $\Phi_{xy}(z)$ is the z-transform of the crosscorrelation function of

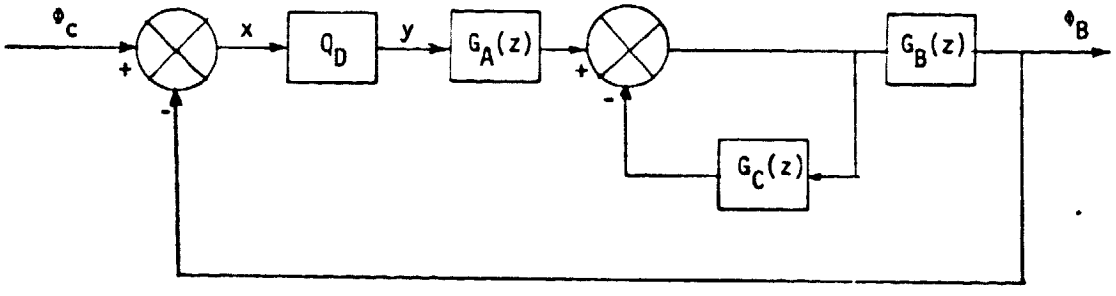

Figure 1-14. Digital LST with quantizer in the displacement channel.

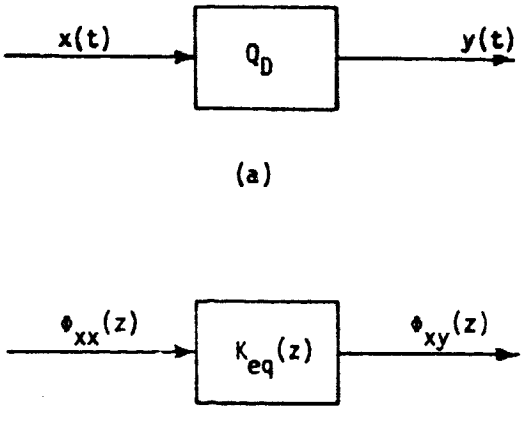

Figure 1-15. The representation of the quantizer with statistical input and output as an equivalent gain.

$x(t)$ and $y(t)$. In order to derive $K_{eq}(z)$, we consider that the input to Q_D is a stationary Gaussian process with zero mean so that the probability function is

$$p(x) = \frac{\exp(-x^2/2\sigma_x^2)}{\sqrt{2\pi}\,\sigma_x} \tag{1-52}$$

where σ_x is the standard deviation of $x(t)$.

The crosscorrelation function of $x(t)$ and $y(t)$ is given by

$$\Phi_{xy}(\tau) = \int_{-\infty}^{\infty} Q_D(\lambda)p(\lambda)\rho\lambda d\lambda \tag{1-53}$$

where

$$Q_D[x(t)] = y(t) \tag{1-54}$$

is the mathematical description of the quantizer, and

$$\rho = \frac{\Phi_{xx}(\tau)}{\sigma_x^2} \tag{1-55}$$

Thus,

$$\Phi_{xy}(\tau) = \frac{1}{\sigma_x^2}\,\Phi_{xx}(\tau) \int_{-\infty}^{\infty} Q_D(\lambda)p(\lambda)\lambda d\lambda \tag{1-56}$$

Taking the z-transform on both sides of Eq. (1-56) and rearranging, we have

$$K_{eq}(z) = \frac{\Phi_{xy}(z)}{\Phi_{xx}(z)} = \frac{1}{\sigma_x^2} \int_{-\infty}^{\infty} Q_D(\lambda)p(\lambda)\lambda d\lambda \tag{1-57}$$

Although the equivalent gain $K_{eq}(z)$ is indicated as a function of z, the nature of the right-hand side of Eq. (1-57) implies that it is always a constant. It is apparent that although our interest is centered on the quantizer nonlinearity, in general, the definition of $K_{eq}(z)$ can be applied to any comman nonlinearities found in control systems.

With reference to the quantizer characteristics of Fig. 1-7,

$$y(t) = 0 \qquad -h/2 < x < h/2$$

$$y(t) = -h \qquad -3h/2 < x \leq -h/2$$

$$y(t) = h \qquad h/2 \leq x < 3h/2$$

$$\vdots$$

$$y(t) = -(N-1)h \qquad -\frac{2(N-1)h}{2} < x \leq -\frac{(2N-3)h}{2}$$

$$y(t) = (N-1)h \qquad \frac{2(N-3)h}{2} \leq x < \frac{(2N-1)h}{2}$$

$$y(t) = -Nh \qquad -\infty < x \leq -\frac{(2N-1)h}{2}$$

$$y(t) = Nh \qquad \frac{2(N-1)h}{2} \leq x < \infty$$

where N is a positive integer.

Equation (1-57) gives

$$K_{eq}(z) = \frac{1}{\sigma_x^2}\left[\int_{-\infty}^{-(2N-1)h/2} (-Nh)p(\lambda)\lambda d\lambda + \int_{-(2N-1)h/2}^{-(2N-3)h/2} -(N-1)hp(\lambda)\lambda d\lambda + \cdots + \int_{-3h/2}^{-h/2} -hp(\lambda)\lambda d\lambda + \int_{h/2}^{3h/2} hp(\lambda)\lambda d\lambda + \cdots + \int_{(2N-3)h/2}^{(2N-1)h/2} (N-1)hp(\lambda)\lambda d\lambda + \int_{(2N-1)h/2}^{\infty} Nhp(\lambda)\lambda d\lambda\right] \qquad (1\text{-}58)$$

Or,

$$K_{eq}(z) = \frac{1}{\sigma_x^2}\left[2h\int_{h/2}^{3h/2} p(\lambda)\lambda d\lambda + \cdots + 2(N-1)h\int_{(2N-3)h/2}^{(2N-1)h/2} p(\lambda)\lambda d\lambda + 2Nh\int_{(2N-1)h/2}^{\infty} p(\lambda)\lambda d\lambda\right] \tag{1-59}$$

Since all the integrals in the last equation have the same integrand, we evaluate one of the integrals as follows:

$$\int_{h/2}^{3h/2} p(\lambda)\lambda d\lambda = \int_{h/2}^{3h/2} \frac{\exp(-\lambda^2/2\sigma_x^2)}{\sqrt{2\pi}\,\sigma_x}\lambda d\lambda \tag{1-60}$$

Let

$$u = \lambda^2/2\sigma_x^2$$

Then

$$du = \frac{\lambda d\lambda}{\sigma_x^2} \qquad \text{or} \qquad \lambda d\lambda = \sigma_x^2\, du$$

and

$$\int_{h/2}^{3h/2} p(\lambda)\lambda d\lambda = \frac{1}{\sqrt{2\pi}}\int_{h^2/8\sigma_x^2}^{9h^2/8\sigma_x^2} \exp(-u)\sigma_x du$$

$$= \frac{1}{\sqrt{2\pi}}\sigma_x\left[\exp\left(-\frac{9h^2}{8\sigma_x^2}\right) + \exp\left(-\frac{h^2}{8\sigma_x^2}\right)\right] \tag{1-61}$$

Thus, the equivalent gain for the quantizer with 2N levels of quantization is

$$K_{eq}(z) = \sqrt{\frac{2}{\pi}}\frac{h}{\sigma_x}\left[\exp\left(-\frac{h^2}{8\sigma_x^2}\right) + \exp\left(-\frac{9h^2}{8\sigma_x^2}\right) + \exp\left(-\frac{25h^2}{8\sigma_x^2}\right) + \cdots + \exp\left(-\frac{(2N-1)^2h^2}{8\sigma_x^2}\right)\right] \tag{1-62}$$

Although the equivalent gain has been derived from Q_D, the response of the closed-loop system of Fig. 1-14 cannot be determined by using $K_{eq}(z)$ directly, since σ_x, the standard deviation, of $x(t)$ is not known. The analysis procedure is outlined as follows:

For a given σ_c, which is the rms value of the input,

(1) The equivalent gain $K_{eq}(z)$ is computed using Eq. (1-62) for various values of σ_x.

(2) The values of σ_x that correspond to the various values of $K_{eq}(z)$ obtained in step (1) are calculated from

$$\sigma_x = \left[\frac{1}{2\pi j}\oint M_x(z)M_x(z^{-1})\Phi_{cc}(z)z^{-1}dz\right]^{1/2} \tag{1-63}$$

where

$$M_x(z) = \frac{1}{1 + K_{eq}(z)G_A(z)G_B(z) + G_c(z)} \tag{1-64}$$

and

$$\Phi_{cc}(z) = \sigma_c^2$$

It is assumed that the input of the system is a white noise. The solution of σ_x for the given σ_c is determined when there is a match between σ_x from Eq. (1-63) and that used in step (1).

(3) The rms attitude response of the system is determined from

$$\sigma_B = \left[\frac{1}{2\pi j}\oint M(z)M(z^{-1})\Phi_{cc}(z)z^{-1}dz\right]^{1/2} \tag{1-65}$$

using the $K_{eq}(z)$ which corresponds to the σ_x obtained in step (2).

For the LST system, a quantization level of h = 0.003 is selected for Q_D. The quantizer is assumed to saturate after 5000 increments; that is, N = 5000 in Eq. (1-62). A digital computer program is prepared which automatically cuts off the series of Eq. (1-62) when an additional term is contributing less than 10^{-6} to the entire result. The sampling period T is chosen to be 25 msec, and the system transfer functions $G_A(z)$, $G_B(z)$, and $G_C(z)$ are given by Eqs. (1-38), (1-36), and (1-37), respectively. Following the procedure outlined above, the results of the analysis with several values of σ_c are tabulated in Table 1-4.

The results in Table 1-4 show that for a given set of quantization and saturation levels, both small and large input signals cause the quantizer to act as an attenuator. The true characteristics of the system as a function of the input σ_c are displayed by normalizing σ_B. The last column in Table 1-4 represents the normalized output σ_{BN}, which is defined as

$$\sigma_{BN} = \frac{\sigma_B}{\sigma_{B1}\sigma_c} \tag{1-66}$$

where

$$\sigma_{B1} = \sigma_B \quad \text{at} \quad \sigma_c = 1 \quad . \tag{1-67}$$

Table 1-4.

Input σ_c	σ_x	K_{eq}	No. of terms used in $K_{eq}(z)$	Output σ_B	Normalized output σ_{BN}
5×10^{-4}	5.318×10^{-4}	0.075	2	5.20×10^{-5}	0.4
10^{-3}	1.086×10^{-3}	0.797	3	2.40×10^{-4}	0.92
10^{-2}	1.093×10^{-2}	1.0	19	2.68×10^{-3}	1.0
10^{-1}	1.093×10^{-1}	1.0	176	2.60×10^{-2}	1.0
1	1.093	1.0	1753	2.60×10^{-1}	1.0
10	10.87	0.836	5000	2.383	0.916
50	53.37	0.22	5000	6.88	0.529

Figure 1-16 shows the plot of $K_{eq}(z)$ versus σ_x. The plot has the significance of a "statistical describing function" of the quantizer. This plot shows that for small inputs, when the input magnitude is comparable to the quantization level, h, the gain drops below unity, and the quantizer is attenuating the signal. For larger inputs the quantizer appears as a unity-gain element in a statistical sense, and for very large inputs, where the input magnitude is comparable to maximum output (N levels of h), the quantizer gain again reduces, and the input is attenuated.

Figure 1-17 gives a plot of σ_x versus σ_c which represents the solution of Eq. (1-63) and step (1) for the range of σ_c considered.

Figure 1-18 shows a plot of σ_{BN} versus σ_c. It is seen that the normalized output reduces from unity in the ranges of σ_c when $K_{eq}(z)$ is less than 1.

As an interesting comparison, the statistical method of Section 1-5 assumes $K_{eq}(z) = 1$ for all values of σ_c and, consequently, it always yields

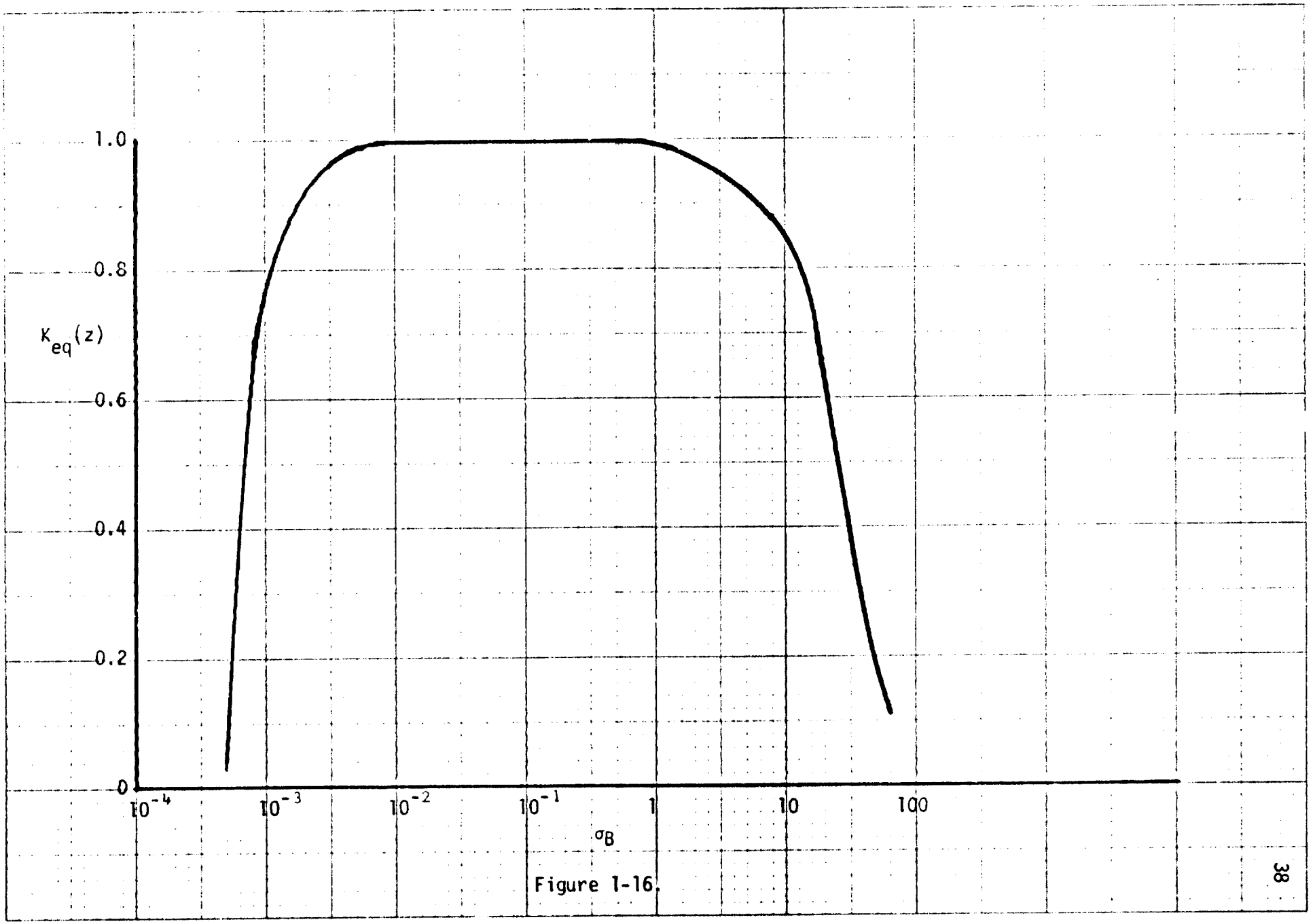

Figure 1-16.

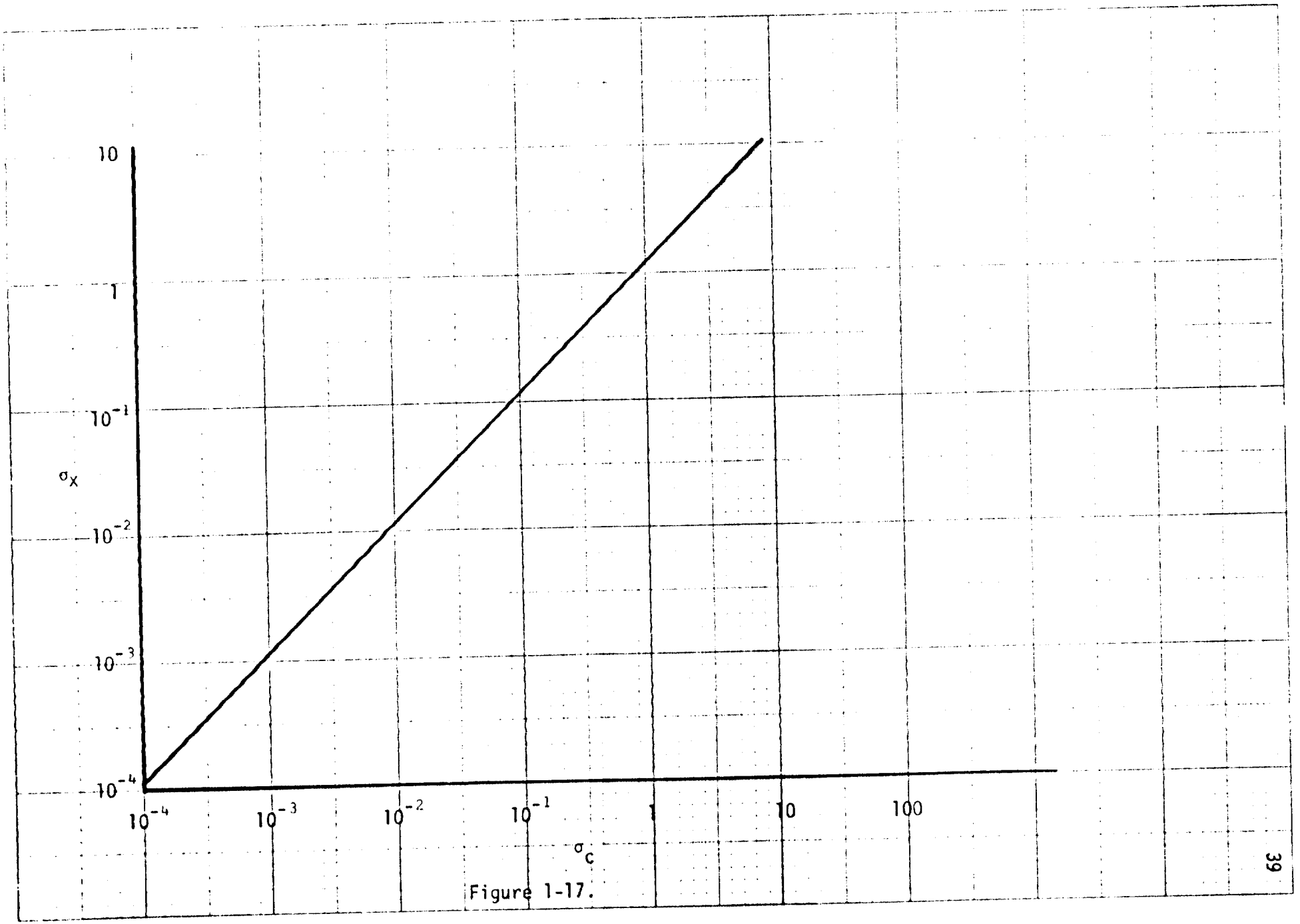

Figure 1-17.

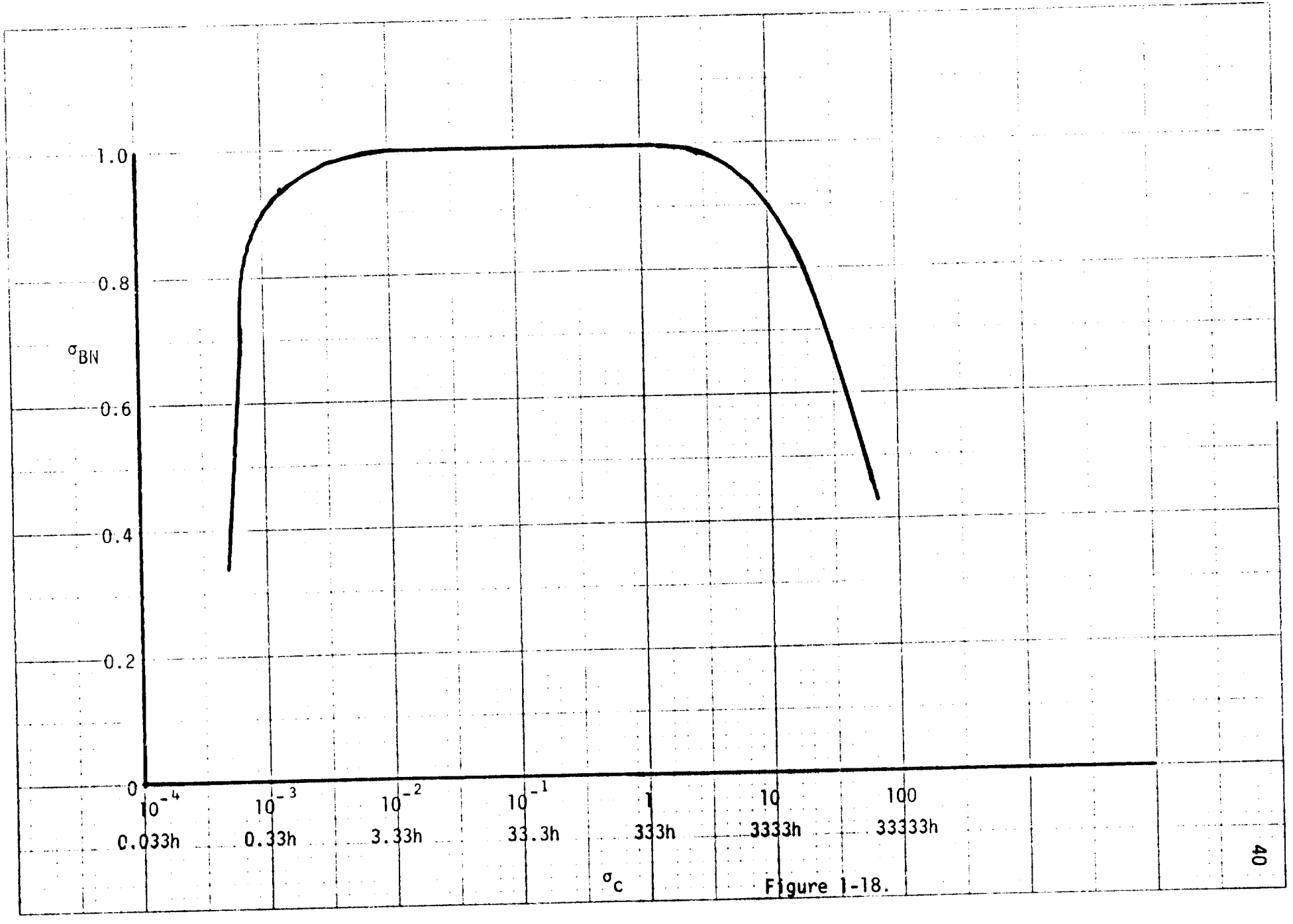
1.0
0.8
σ_{BN}
0.6
0.4
0.2
0
10^{-4}
0.033h
10^{-3}
0.33h
10^{-2}
3.33h
10^{-1}
33.3h
1
333h
10
3333h
100
33333h
σ_c

Figure 1-18.

a result of $\sigma_{BN} = 1$. In this sense that method is more conservative and does not recognize the severity of the nonlinearity due to the quantizer at very small and very large input magnitudes.

REFERENCES

1. K. Frevert and R. Joyce, "Pointing Stability of A Fine Pointing Control System For A Low-Cost LST With A Reaction Wheel Model And Dahl Nonlinearity," Northrop Services, Inc., Memorandom No. 9250C-74-51, December 20, 1974.

2. K. Frevert and R. Joyce, "Effects of Dahl Nonlinear Friction Model On Pointing Stability," Northrop Services, Inc., Memorandom No. 9250C-75-10, January 28, 1975.

3. R. W. Troop, "An Equivalent Gain Analysis of Nonlinear Sampled-Data Systems Subjected to Stochastic Inputs," M.S. Thesis, Air University, USAF, Wright-Patterson AFB, Ohio, 1968.

4. R. F. Prueher, "An Equivalent Gain and Stochastic Analysis For Nonlinear Sampled-Data Control Systems," Ph.D Thesis, Department of Electrical Engineering, University of Illinois, Urbana, Illinois, 1966.

END

DATE

FILMED

JUN 16 1975